Proceedings of ISFOG 2025
5TH INTERNATIONAL SYMPOSIUM ON
FRONTIERS IN OFFSHORE GEOTECHNICS
Nantes, France | June 9-13 2025

ISBN 978-2-85782-758-0

Geometrical optimization of extendable plate anchor for floating offshore wind through 1G model test

Shun Nomura*
Tokyo University of Marine Science and Technology, Tokyo, Japan
Kazuo Tani
Tokyo University of Marine Science and Technology, Tokyo, Japan
Nallathamby Sivasithamparam
Norwegian Geotechnical Institute, Oslo, Norway
**nomura.shun@kaiyodai.ac.jp (corresponding author)*

ABSTRACT: This paper introduces a new type of anchor and its geometrical optimization for floating offshore wind, which is named the Extendable plate anchor (ExPLA). This ExPLA extends in the ground pulled from the originally installed position and consists of two plates with a hinge connecting them. To evaluate the feasibility of the expandability of ExPLA, a series of model tests using a miniature anchor model were conducted. A ~1/100 scale anchor model which is 10-20 mm in width, 40mm in height, and 40 mm in length, with two plates connected by a hinge is embedded in the ground in the folded state and then pulled upward. Through these experiments, it was found that the anchor expands as the pull-out length increases. With the help of the index matching method, this extension process was visually observed. Through image analysis, the deployment angle of ExPLA was quantified, and the influence of two geometric parameters, the back slope angle and the dip angle, on the anchor's expandability is evaluated. It was found that the back slope angle is the most dominant parameter in controlling expandability. As the dip angle increases, the pull-out length required for deployment decreases.

Keywords: Expandable Plate Anchor, Plate Anchor, Refractive index matching, Floating Offshore Wind, Laboratory Test

1 INTRODUCTION

Due to the global trend toward the decarbonization, there is a strong demand for offshore wind power. To keep up with this trend, the offshore floating system is key, since over 80 % of the world's wind resources are located offshore at depths greater than 60 m（Musial et al., 2020). At such depth, floating systems offer economic and technological advantages compared to the fixed bottom (Myhr et al., 2014). Based on this background, there is a strong demand for an anchoring system that is easy to install and generates high resistance forces during operation. Several types of anchoring systems exist such as pile anchors, suction caissons, drag embedment anchors (DEA), vertical loaded anchors (VLA), and, dynamically installed anchors (DIA). Some of them are already used on-site (e.g., Frankenmolen et al., 2017: Richardson, 2008;

	Anchor type	Pile Anchor	Suction anchor	DEA	VLA	DIA
Technological aspect	Anchoring potential	High	High	Low	Low	Low
	Load path angle	Any angle	Any angle	Horizontal	Vertical	Any angle
	Installation accuracy	Precise	Precise	Not precise	Not precise	Precise
Economical aspect	Manufacturing cost	High	High	Low	Low	Low
	Installation vessel	Large	Large	Small	Small	Small
	Management cost	Low	Low	High	High	High
Ecological aspect	Noise in installation	Noise from hammer	Low noise	Low noise	Low noise	Low noise
	Recoverability	Recoverable	Recoverable	Recoverable	Recoverable	Non-recoverable

Table 1 Features of existing anchoring technology

Houlsby and Byrne, 2005; Byrne and Houlsby, 2015; Ullah et al., 2023). Table 1 summarises the features of existing anchors based on technological, economical, and ecological aspects. As reported by ORE Catapult and ARUP (2024), several anchoring technologies exists, and their suitability should be assessed based on the specific requirements and limitations, considering factors such as installation, manufacturing, and operation. There is also a need for innovative anchoring solutions that address these logistical, economic and environmental challenges to support the successful development of commercial-scale wind farms.

Based on this background, in this study, we introduce a new type of anchor concept, called the Expandable Plate Anchor (ExPLA). As shown in Figure 1, ExPLA consists of two plates and a hinge, and installed in the folded state in the ground. Then, by pulling the hinge upward, it expands and enlarges the horizontal area to receive the resistance for anchoring.

In this study, the applicability of the anchor is discussed through 1G model test. The expansion process is tracked with the help of the refractive index matching method and image analysis. Then, its expandability in relation to geometry is evaluated based on the experimental results.

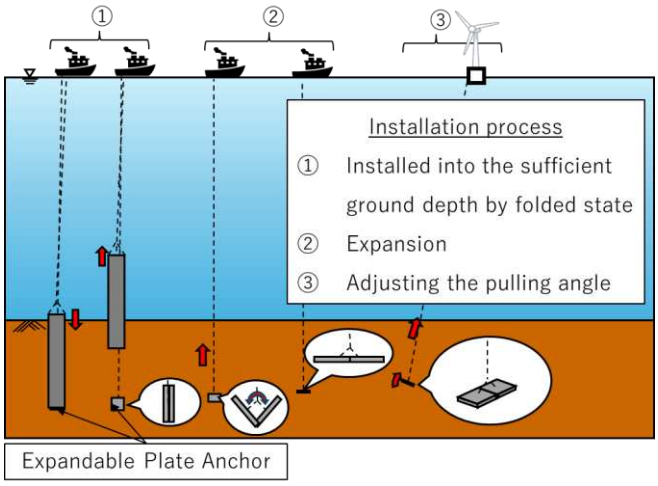

Figure 1 The concept of the ExPLA

2 EXPERIMENTAL METHOD

2.1 Experimental apparatus

Figure 2 represents the experimental apparatus. In this setup, the anchor is suspended by the stainless rod connected to a load cell and an actuator at the top of frame. The expanding process with upward motion are recorded by a digital camera (SONY, DSC RX 100 III) and a laser displacement analyser (KEYENCE, IL-600). At the bottom of the loading frame, the model ground is placed in the acrylic box. The miniature anchor model, designed as in Figure 3, has a specific geometry for expansion and was manufactured using a 3D printer. The thickness, width, and height of the anchor's geometry was 10-20, 40, and 40 mm, respectively. Its size corresponds to approximately ~1/100 of on-site scale. To define the anchor's

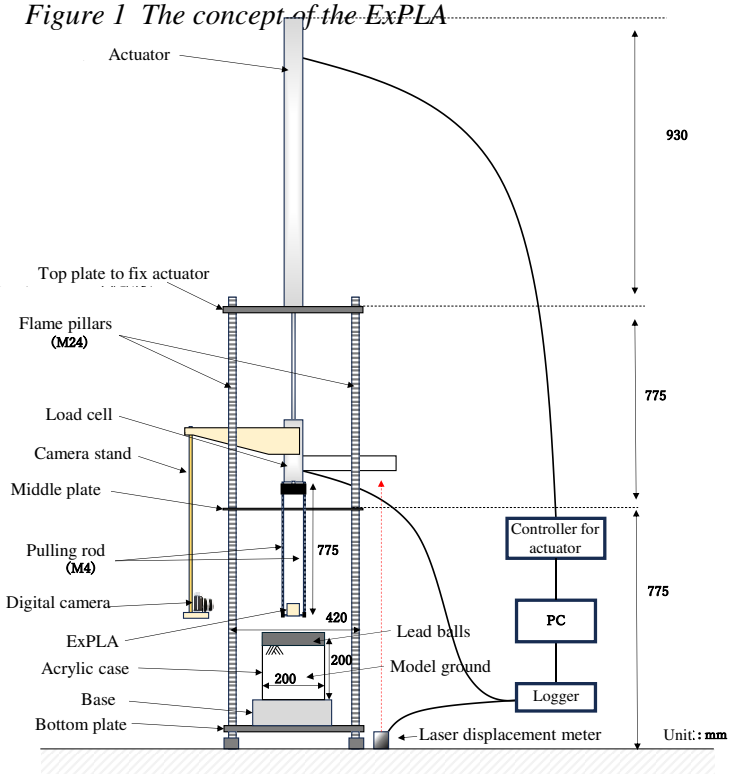

Figure 2 Experimental setup

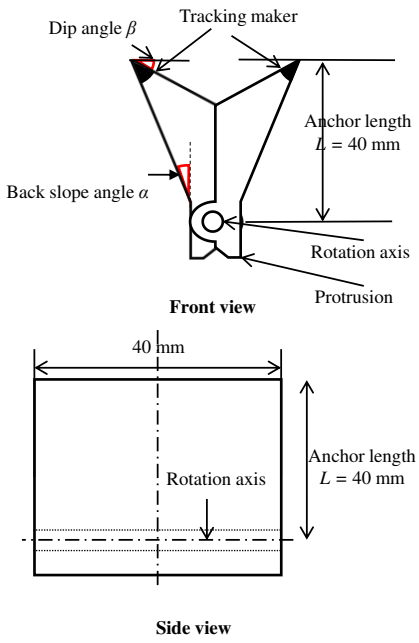

Figure 3 Anchor geometry

geometry, two parameters α and β are introduced, representing the back slope angle and the dip angle, respectively. To prevent the deployment angle θ from exceeding 180°, small protrusion are installed at the bottom of the anchor as a stopper.

2.2 Ground Material

To observe the upward and expanding motions of the anchor, the reflective index matching method is applied to the model ground (e.g., Iskander, 2015: Mahmoud, 2011). The transparent fused silica particles, whose mean diameter of D_{50} = 1.36 mm and density ρ_s = 2.2 Mg/m^3 are used. The particle size distribution and material properties are presented in Figure 4 and Table 2, respectively. Silicon oil, with a refractive index n =1.45 at 22 °C, is used as the pore fluid. By carefully mixing these materials and avoiding contamination by the trapped air, the ground becomes transparent.

Before the experiment, the saturated ground material is filled up to 10 mm from the bottom. Then, the anchor is installed in the folded state, positioning it at the desired location in the ground. Next, the model ground is prepared by layering the material in four stages, up to a total thickness of 140 mm. The ground is carefully layered to keep the transparency in the area. The density of the ground is controlled by the material weight to achieve relative density Dr =70 %. After preparing the model ground, lead spheres are placed on its surface to apply an equivalent overburden pressure corresponding to the initial ground height of D_0 = 1000mm. As a result, the vertical effective stress of the hinge is 17 kN/m^2. The normalized depth of the anchor length is D_0/L =25, which is relatively deep compared to the real-world operations.

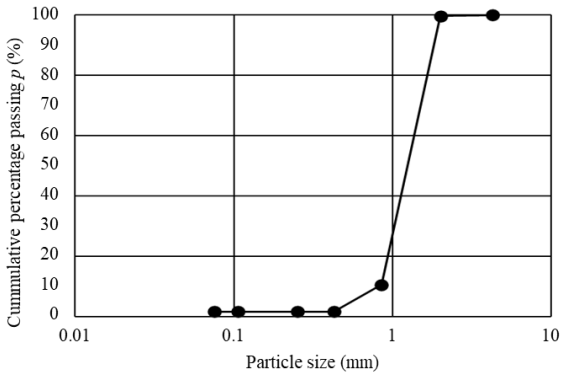

Figure 4 particle size distribution

Table 2 Physical parameter of particle

Maximum dry unit density ρ_{dmax} (Mg/m^3)	1.33
Minimum dry unit density ρ_{dmin} (Mg/m^3)	1.14
Uniformity coefficient U_c	1.81
Angle of repose ϕ_{res} (°)	37

2.3 Experimental procedure and test cases

A series of experiment were conducted. The upward velocity of the anchor was fixed at 0.1 mm/s to prevent the generation of excessive pore fluid pressure and to minimize the dependency on pullout speed. The experiments are repeated three times for each case. The test cases are presented in Table 3.

Table 3 Test cases

Back slope angle α (°)	**Dip angle β(°)**
5	0
10	0
20	0
	10
	20
	40

3 EPERIMENTAL RESULT

3.1 Typical result

Figure 5 show the snapshots every 20 mm from the pullout distance d = 0 to 60 mm in case of α = 20° and β = 40°. Figure 6 presents the relationship between θ and d. θ is measured by tracking the edges of the anchor with a help of the image analysis. After the hinge is pulling upward, the anchor begins to open, and θ continuously increases. θ reaches θ_{max} = 180° in d = 50 mm. The length required for the anchor to fully open is defined as d* and, in this case, it is d* = 1.3L.

3.2 Dependency on α

Figure 7 represents the results of α = 5, 10, and 20 when β is fixed to 20°. Increase in θ accompanies the increase in d for all cases. The incremental rate of θ with respect to d (i.e., dθ/dd) increases as α increases. In the cases of α = 10 and 20°, θ reaches θ_{max} =180° and d*= 80 and 68 mm, respectively. However, for α = 5°, θ reaches θ_{max} =160° (less than 180°) at d* = 85-90 mm. These result indicates that the value of α is dominant parameter controlling whether the anchor deploys or not.

3.3 Dependency on β

Figure 8 presents d - θ relation in case of β = 5, 10, 20, and 40° when α is fixed at 20°. In all cases, the anchor fully extends (i.e., θ_{max} > 160°) by d = 70 mm. As β increase from 0° to 40°, the incremental rate dθ /dd increasees, while d* decreases from 68 to 50 mm.

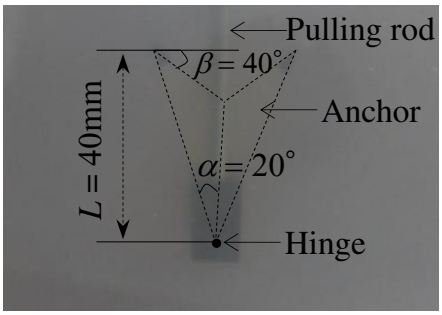

d = 0 mm

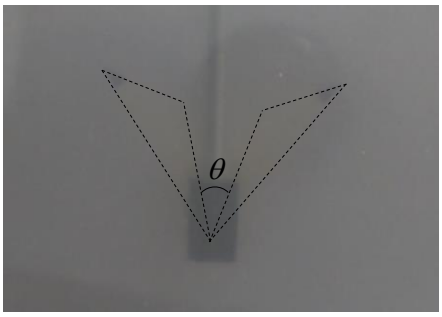

d = 20 mm

d = 40 mm

d = 60 mm

Figure 5 Snapshot of the experiment

Although d* decrease as β increase, this trend appears to be limited, as the rate of decrease in d* slows with increasing β increases. Therefore, the effect of β is smaller than that of α.

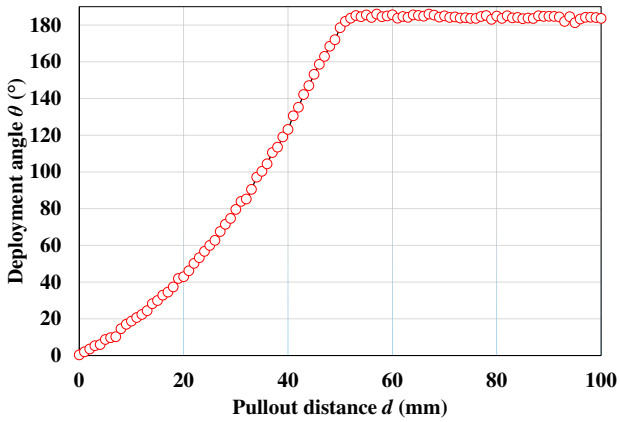

Figure 6 d - θ relation in case of α =20°, and β =40°

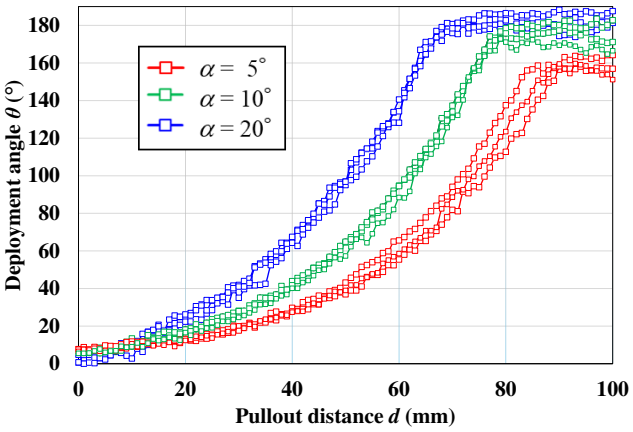

Figure 7 d - θ relation in case of α =5,10, 20°, and β =0°

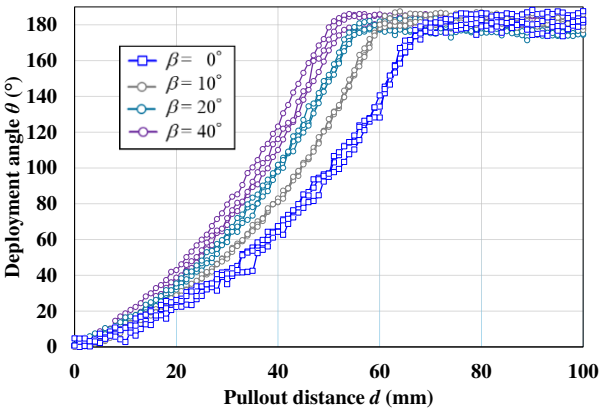

Figure 8 d - θ relation in case of α = 20°, and β =0, 10, 20, 40°

4 DISCUSSION

Figure 9 and 10 present the value of d^*/L as a function of α and β, respectively. Here, d^* is defined as the point where $d\theta/dd < 1°$ /mm and $\theta > 150°$. Each point represents the averaged value for each case. For α, d^*/L significantly decreases from 2.1 to 1.7 as α increases from 0 to 20°. This trend accelerates with increasing α, indicating that the anchor's area receives sufficient rotational moment for deployment as α increases.

For β, it is also effective in reducing d^*/L. d^*/L decreases from 1.7 to 1.3 as β increases to 40°. However, this trend decelerates as β increases, which is the opposite trend observed for α.

From the engineering point of view, the horizontal projected area of the anchor should be as small as possible to allow instalation. Meanwhile, a smaller pullout length is preferable for deployment. Thereby, α should be larger than a minimum threshold to ensure deployment in the anchor design. On the other hand, β does not significantly affect the projected area. Instead, it provides the local and/or minor geometrical advantage for anchor deployment. As a result, its effect is limited and will eventually reach saturation.

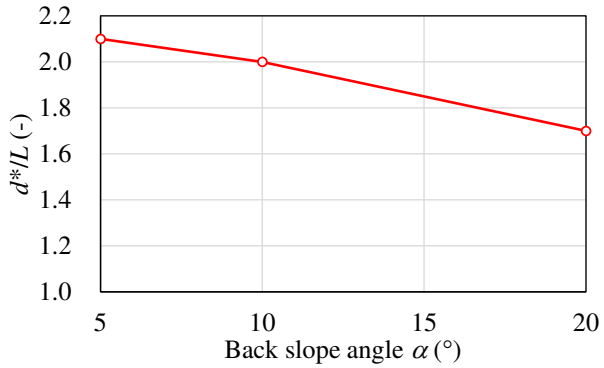

Figure 9 α - d^*/L relation in case of α =5,10, 20°, and β =0°

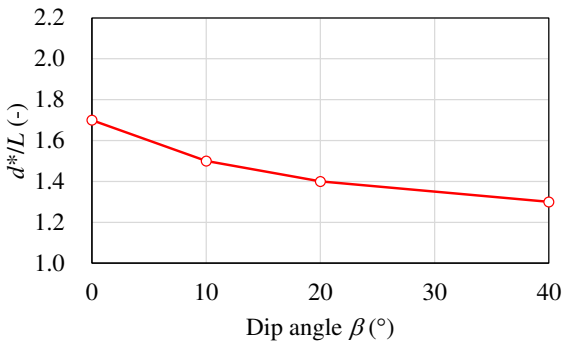

Figure 10 β - d^*/L relation in case of α =0,10, 20, 40°, and α =20°

5 CONCLUSION

In this paper, the concept of a new anchoring system, ExPLA, is introduced for floating offshore wind. ExPLA is composed of two plates connected a hinge, allowing it to be installed in the ground in a folded state, which reduces the horizontal area. This mechanical characteristic may provide a significant advantage in offshore construction. In addition, ExPLA is designed to expand in the ground when pulled upward. Then it enlarges its horizontal projected area. This unique mechanism offers advantages in both the installation and operation stage of floating offshore wind.

To validate the concept on ExPLA, 1G model test were conducted as a first step in a feasibility study. By applying the index matching method, the opening process during pull-out was directly observed, and the relationships between θ and d are summarized according to α and β.

Although the study is still in its preliminary stage, two main findings for practical viability in real-world applications were obtained through the experiments:

1. The back slope angle α is a dominant parameter controlling expandability by generating the rotational moment for opening and the loss of embedment depth of d^*.
2. The dip angle β plays a limited but supportive roll in reducing d^*.

AUTHOR CONTRIBUTION STATEMENT

First Author: Data curation, Formal Analysis, Writing- Original draft. **Other Authors**.: Conceptualization, Methodology, Supervision.

ACKNOWLEDGEMENTS

The authors thank Arata Sato for his assistance in conducting the experiments and analysing the data on this research. This work was supported by a Fusion Oriented Research for disruptive Sisense and Technology (JPMJFR205U) from Japan Science and Technology Agency (JST) and Grant-in-Aid for Sor Scientific Research (C) (22K04306) from the Japan Society for the Promotion of Science (JSPS). We would like to thank the two anonymous reviewers for their thoughtful and detailed feedback. Their suggestions were instrumental in strengthening our manuscript, and we truly appreciate their time and effort.

REFERENCES

Myhr, A., et al. (2014). Levelised cost of energy for offshore floating wind turbines in a life cycle perspective. Renewable Energy, 66, 714-728.

Musial, W., et al. (2020). Offshore Wind Market Report: 2020 Edition. U.S. Department of Energy.

Frankenmolen, S., Erbrich, C. T., Fearon, R. 2017. Successful installation of large suction caissons and driven piles in carbonate soils. In Proceedings of 8th International Conference on Offshore Site Investigation and Geotechnics. Society for Underwater Technology, London, UK. 539–548, https://doi.org/10.3723/OSIG17.539.

Richardson, B, E. 2008. Dynamically Installed Anchors for Floating Offshore Structures. PhD thesis, The University of Western Australia, Perth, Australia.

Houlsby, G. T., Byrne, B. W., 2005. UK design procedures for installation of suction caissons in clay and other materials. Proceedings of the Institution of Civil Engineers – Geotechnical Engineering 158(2): 75–82, https://doi.org/10.1680/geng.2005.158.2.75.

Byrne, B, W., Houlsby, G, T. 2015. Helical piles: an innovative foundation design option for offshore wind turbines. Philosophical Transactions: Mathematical, Physical and Engineering Sciences 373(2035): 20140081, https://doi.org/10.1098/rsta.2014.0081.

Ullah, S, N., O'Loughlin, C., Hu, Y., Hou, L. F. 2023. Torsional installation and vertical tensile capacity of helical piles in clay. Géotechnique, https://doi.org/10.1680/jgeot.22.00014.

ORE Catapult, and ARUP. 2024. Floating Offshore Wind Anchor Review: Public Summary Report. PN000585-RPT-005 - Rev. 01. Floating Offshore Wind Centre of Excellence.

Iskander, M., Bathurst, R. J., Omidvar, M. 2015. Past, Present, and Future of Transparent Soils. ASTM International. Geotechnical Testing Journal 38(5), 557–573, https://doi.org/10.1520/GTJ20150079

Mahmoud, A. 2011. Analysis of Tunneling-Induced Ground Movements Using Transparent Soil Models. Journal of Geotechnical and Geoenvironmental Engineering 137 (5): 525-535, https://doi.org/10.1061/(ASCE)GT.1943-5606.0000456